CONF-821101--15

CONF-821101--15

DE83 003486

APPLICATIONS OF ENERGY-RELEASE-RATE TECHNIQUES TO PART-THROUGH CRACKS IN EXPERIMENTAL PRESSURE VESSELS*

B. R. Bass
Computer Sciences

R. H. Bryan
J. W. Bryson
J. G. Merkle
Heavy Section Steel Technology Program
Oak Ridge National Laboratory

Paper to be submitted for consideration at the Fracture Mechanics Session of the American Society of Mechanical Engineers Winter Annual Meeting in Phoenix, Arizona

November 14-19, 1982

*Based on work performed by Union Carbide Corporation, Nuclear Division, for the U. S. Department of Energy under U. S. Government Contract W-7405 eng 26.

APPLICATIONS OF ENERGY-RELEASE-RATE TECHNIQUES TO PART-THROUGH CRACKS IN EXPERIMENTAL PRESSURE VESSELS

B. R. Bass
Computer Sciences
Union Carbide Corporation-Nuclear Division
Oak Ridge, Tennessee

R. H. Bryan
J. W. Bryson
J. G. Merkle
Heavy Section Steel Technology Program
Oak Ridge National Laboratory
Oak Ridge, Tennessee

ABSTRACT

In nonlinear applications of computational fracture mechanics, energy release rate techniques are used increasingly for computing stress intensity parameters of crack configurations. Recently, deLorenzi used the virtual-crack-extension method to derive an analytical expression for the energy release rate that is better suited for three-dimensional calculations than the well-known J-integral. Certain studies of fracture phenomena, such as pressurized-thermal-shock of cracked structures, require that crack tip parameters be determined for combined thermal and mechanical loads. A method is proposed here that modifies the isothermal formulation of deLorenzi to account for thermal strains in cracked bodies. This combined thermo-mechanical formulation of the energy release rate is valid for general fracture, including nonplanar fracture, and applies to thermo-elastic as well as deformation plasticity material models. Two applications of the technique are described here. In the first, semi-elliptical surface cracks in an experimental test vessel are analyzed under elastic-plastic conditions using the finite element method. The second application is a thick-walled test vessel subjected to combined pressure and thermal shock loading.

NOMENCLATURE

- A - Crack face area
- a - Crack depth
- b - Half-length of surface crack
- C - Surface domain
- E - Elastic modulus
- F_α - Components of surface traction
- f_α - Components of body force
- G_τ - Energy release rate, equation (12)
- G^* - Energy release, equation (11)
- h - Heat transfer coefficient
- J_α - Components of J-integral, equation (18)
- J_A - Applied J, a function of geometry and applied load
- J_{Ic} - Critical J for fracture initiation, a material property
- J_R - Tearing resistance, a material property
- K_I - Stress intensity factor (mode I)
- n_α - Components of unit normal
- p - Internal pressure
- r - Radial coordinate, measured from crack tip
- S - Surface domain
- T - Temperature
- t - Time
- u_α - Components of surface displacement
- u^m_α - Components of interior displacement
- V - Volume domain
- W - Strain energy density function
- w - Plate width or wall thickness
- x_α - General spatial coordinates

GREEK SYMBOLS

- α - Thermal expansion coefficient
- $\delta_{\alpha\beta}$ - Kronecker delta
- Δ - Incremental change in kernel
- $\varepsilon_{\alpha\beta}$ - Components of total strain
- $\varepsilon'_{\alpha\beta}$ - Components of mechanical strain
- ε_h - Hoop strain
- $\hat{\varepsilon}_{\alpha\beta}$ - Components of thermal strain
- $\sigma_{\alpha\beta}$ - Components of stress
- σ_y - Yield stress in uniaxial tension
- ν - Poisson's ratio
- θ - Elliptic angle

SUBSCRIPTS

- I, II - Volume or surface sub-domain
- α, β, γ, δ - Component indices (range 1, 2, 3)

INTRODUCTION

Nonlinear methods in computational fracture mechanics have focused increasingly on energy release rate techniques for computing stress intensity parameters of crack configurations. For two-dimensional (2-D) problems, the path-independent J-integral (1) is conveniently used to compute energy release rates for linearly elastic and deformation plasticity material models. However, the extension of the J-integral to three dimensions is unwieldy because of the necessity of evaluating the J-function over defined surfaces in three-dimensional (3-D) space. A method better suited for 3-D calculations is the virtual-crack-extension technique, introduced by Hellen (2) and Parks (3) in the context of finite elements. The formulations of Hellen and Parks were based on calculations of the energy released when a crack front in a finite element model is given a virtual displacement to simulate crack extension. Recently, deLorenzi (4) used the virtual extension method and continuum theory to derive an analytical expression for the energy release rate that is not tied to a particular numerical technique. The formulation is valid for general isothermal fracture behavior, including nonplanar fracture, and applies to elastic as well as deformation plasticity material models. In applications, deLorenzi (5,6) used the finite element method to evaluate the energy release rate function.

Certain studies of fracture phenomena, such as those associated with pressurized-thermal-shock (7), require that crack tip stress intensity parameters be determined for cracked structures subjected to combined thermal and mechanical loads. A method is proposed here that modifies the isothermal formulation of deLorenzi to account for thermal strains in cracked bodies. The modification is strictly valid for hyperelastic materials, but an approximation to incremental thermo-elastic-plastic theory can be achieved provided there is no unloading and the departure from a radial stress path is not severe. This thermo-mechanical formulation of the energy release rate is used also to deduce the modified three-dimensional J-integral expression applicable to thermally-strained bodies containing planar cracks. The modified J-integral presented here represents a generalization of the expressions derived previously by Ainsworth et al (8) and by Wilson and Yu (9) for thermal applications.

The following section presents a summary of the virtual-crack-extension technique that incorporates the proposed thermal strain modifications, along with corresponding changes in the J-integral development. For brevity, only the essential alterations to deLorenzi's argument are treated here; the reader is directed to appropriate references for additional details. This is followed by two applications of the technique to crack configurations in pressure vessels. In the first application, semi-elliptical surface cracks in an experimental test vessel were analyzed under elastic-plastic conditions. Three-dimensional finite element analyses were performed for a family of crack configurations and internal pressures using a deformation plasticity material model. The second application is a cylindrical test vessel subjected to combined pressure and thermal shock loading. Two-dimensional finite element analyses were performed on surface cracks using both the virtual-crack-extension and the J-integral techniques. To evaluate the conclusions derived from the two-dimensional results, analyses were also performed on three-dimensional models of the crack configurations.

ENERGY RELEASE RATE CALCULATIONS

Griffith (10,11) first suggested a thermodynamic criterion for fracture by considering the change in energy of a cracked body as the crack length was increased. The energy based argument presented here follows that of deLorenzi (4), but is modified to include the effects of thermal strains. The method requires calculation of the released energy G^* corresponding to a small crack advance in a cracked body subjected to surface tractions F_α, body force f_α, and temperature distribution T (see Figure 1). Points of configuration I (prior to crack advance) are mapped into configuration II (after crack advance) by the mapping

$$\bar{x}_\alpha = x_\alpha + \Delta x_\alpha(x_\beta) \tag{1}$$

where x_α, $\bar{x}_\alpha$ correspond to configurations I, II, respectively, and Δx_α is the incremental change in coordinates.

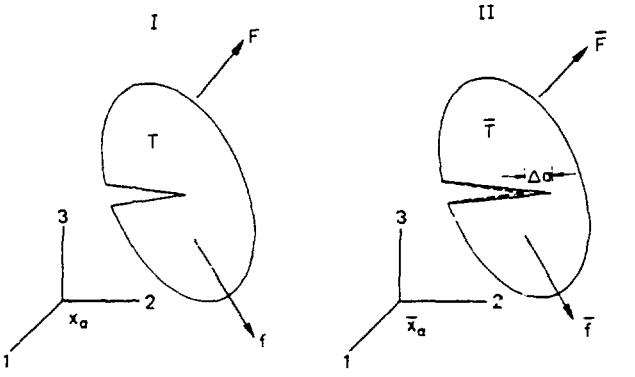

Fig.1 Crack configuration before and after crack extension

The energy release G^* due to the virtual extension Δx_α is the difference of the work of the external forces and the change in strain energy,

$$G^* = \int_S F_\alpha \Delta u_\alpha dS + \int_V f_\alpha \Delta u_\alpha^m dV - \left(\int_{\bar{V}} \bar{W} d\bar{V} - \int_V W dV \right) \quad .$$

In Eq. (2), the strain energy density W is given by

$$W = \int_0^{\varepsilon'_{\gamma\delta}} \sigma_{\alpha\beta} d\varepsilon'_{\alpha\beta} \quad , \tag{3}$$

$$\varepsilon'_{\alpha\beta} = \varepsilon_{\alpha\beta} - \hat{\varepsilon}_{\alpha\beta} \quad , \tag{4}$$

where the mechanical strain components $\varepsilon'_{\alpha\beta}$ are defined in terms of the total strains $\varepsilon_{\alpha\beta}$ and the strains of

free thermal expansion $\hat{\theta}_{\alpha\beta}$. In addition, $\sigma_{\alpha\beta}$ are the components of the stress tensor, Δu_α and Δu^m_α the surface and interior displacement increments, dS and dV the surface and volume differentials.

The strain energy density in configuration II can be written as

$$\bar{W}\Big|_{\bar{x}_\alpha} = W\Big|_{x_\alpha} + \frac{\partial W}{\partial \epsilon'_{\alpha\beta}} \Delta\epsilon'_{\alpha\beta}$$

$$= W\Big|_{x_\alpha} + \frac{\partial W}{\partial \epsilon'_{\alpha\beta}} (\Delta\epsilon_{\alpha\beta} - \Delta\hat{\theta}_{\alpha\beta}) \quad , \qquad (5)$$

where Eq. (4) has been used. The increment in thermal strains is related to the incremental change in coordinates by

$$\Delta\hat{\theta}_{\alpha\beta} = \frac{\partial\hat{\theta}_{\alpha\beta}}{\partial x_\delta} \Delta x_\delta \quad , \qquad (6)$$

and, for a hyperelastic body,

$$\sigma_{\alpha\beta} = \frac{\partial W}{\partial \epsilon'_{\alpha\beta}} \quad . \qquad (7)$$

The following relations from deLorenzi (4) remain valid in the presence of thermal strains:

$$\Delta\epsilon_{\alpha\beta} = \frac{1}{2}\left(\frac{\partial\Delta u_\alpha}{\partial x_\beta} + \frac{\partial\Delta u_\beta}{\partial x_\alpha}\right)$$

$$- \frac{1}{2}\left(\frac{\partial u_\alpha}{\partial x_\delta}\frac{\partial\Delta x_\delta}{\partial x_\beta} + \frac{\partial u_\beta}{\partial x_\delta}\frac{\partial\Delta x_\delta}{\partial x_\alpha}\right) \quad , \qquad (8)$$

$$d\bar{V} \approx \left(1 + \frac{\partial\Delta x_\alpha}{\partial x_\alpha}\right) dV \quad , \qquad (9)$$

$$\Delta u^m_\alpha = \Delta u_\alpha - \frac{\partial u_\alpha}{\partial x_\delta}\Delta x_\delta \quad . \qquad (10)$$

When Eq. (2) is combined with Eqs. (3)-(10) and the equilibrium equations $\sigma_{\alpha\beta,\beta} = -f_\alpha$, with retention of only lower order terms, the energy release parameter G* becomes

$$G^* = \int_V \left(\sigma_{\alpha\beta}\frac{\partial u_\alpha}{\partial x_\delta} - W\delta_{\delta\beta}\right)\frac{\partial\Delta x_\delta}{\partial x_\beta} dV$$

$$+ \int_V \left(\sigma_{\alpha\beta}\frac{\partial\hat{\theta}_{\alpha\beta}}{\partial x_\delta} - f_\alpha\frac{\partial u_\alpha}{\partial x_\delta}\right)\Delta x_\delta dV \quad . \qquad (11)$$

In the absence of thermal strains, Eq. (11) for released energy reduces to the isothermal form of deLorenzi.

The total energy release rate G_T is given by

$$G_T = G^*/\Delta A \qquad (12)$$

where ΔA is the area increment covered by the virtual-crack-extension (see Figure 2). Average and local values of G_T are evaluated, respectively, from uniform and local virtual extensions of the crack front.

Eq. (11) for the energy release G* can be used to derive a modified form of the 3-D J-integral that is valid in the presence of thermal strains. For the 3-D planar crack depicted in Figure 3, let $\Delta x_\delta = \Delta a_\delta$, a constant, in region II surrounding the crack tip; thus $\frac{\partial\Delta x_\delta}{\partial x_\beta} = 0$ in V_{II}. If the region external to V_{II} is denoted V_I, the released energy G* of Eq. (11) can be written

$$G^* = \int_{V_I} \left(\sigma_{\alpha\beta}\frac{\partial u_\alpha}{\partial x_\delta} - W\delta_{\delta\beta}\right)\frac{\partial\Delta x_\delta}{\partial x_\beta} dV$$

$$+ \int_{V_I} \left(\sigma_{\alpha\beta}\frac{\partial\hat{\theta}_{\alpha\beta}}{\partial x_\delta} - f_\alpha\frac{\partial u_\alpha}{\partial x_\delta}\right)\Delta x_\delta dV$$

$$+ \int_{V_{II}} \left(\sigma_{\alpha\beta}\frac{\partial\hat{\theta}_{\alpha\beta}}{\partial x_\delta} - f_\alpha\frac{\partial u_\alpha}{\partial x_\delta}\right)\Delta x_\delta dV \quad . \qquad (13)$$

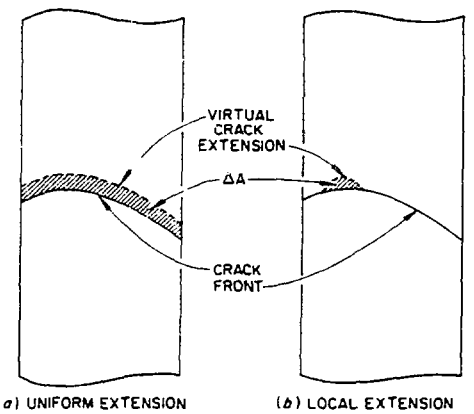

Fig.2 Virtual crack extension for calculating energy release rate G_T for (a) uniform extension and (b) local extension

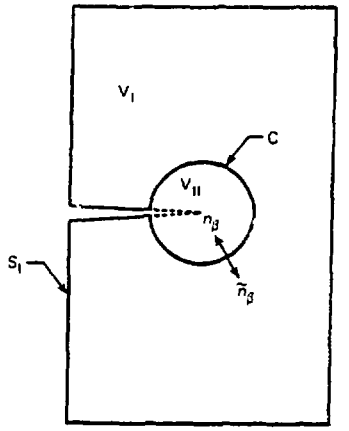

Fig.3 Section normal to crack front showing regions used to calculate G*

When integration by parts and the divergence theorem are applied to the first volume integral, Eq. (13) becomes

$$G^* = \int_{S_I} \left(\sigma_{\alpha\beta} \frac{\partial u_\alpha}{\partial x_\delta} - W\delta_{\delta\beta} \right) \Delta x_\delta n_\beta dS$$

$$- \int_{V_I} \left[\left(\sigma_{\alpha\beta,\beta} \frac{\partial u_\alpha}{\partial x_\delta} + \sigma_{\alpha\beta} \frac{\partial^2 u_\alpha}{\partial x_\delta \partial x_\beta} - \frac{\partial W}{\partial x_\delta} \right) \Delta x_\delta \right.$$

$$\left. - \left(\sigma_{\alpha\beta} \frac{\partial \hat{\theta}_{\alpha\beta}}{\partial x_\delta} - f_\alpha \frac{\partial u_\alpha}{\partial x_\delta} \right) \Delta x_\delta \right] dV$$

$$+ \int_{V_{II}} \left(\sigma_{\alpha\beta} \frac{\partial \hat{\theta}_{\alpha\beta}}{\partial x_\delta} - f_\alpha \frac{\partial u_\alpha}{\partial x_\delta} \right) \Delta x_\delta dV \quad , \qquad (14)$$

where S_I is the surface of region I, including surface C, which separates regions I and II. In Eq. (14), the volume integral over V_I is identically zero because of the equilibrium equations and the relations

$$\varepsilon_{\alpha\delta} = \frac{1}{2} \left(\frac{\partial u_\alpha}{\partial x_\beta} + \frac{\partial u_\beta}{\partial x_\alpha} \right) \qquad (15)$$

and

$$\frac{\partial W}{\partial x_\delta} = \frac{\partial W}{\partial \varepsilon_{\alpha\beta}} \frac{\partial \varepsilon_{\alpha\beta}}{\partial x_\delta}$$

$$= \sigma_{\alpha\beta} \frac{\partial^2 u_\alpha}{\partial x_\beta \partial x_\delta} - \sigma_{\alpha\beta} \frac{\partial \hat{\theta}_{\alpha\beta}}{\partial x_\delta} \quad . \qquad (16)$$

DeLorenzi (4) assumes that one or a combination of the following conditions holds on S_I excluding C: $\Delta x_\delta = 0$; $\sigma_{\alpha\beta} n_\beta = 0$; or $\sigma_{\alpha\gamma} n_\gamma \left(\frac{\partial u_\alpha}{\partial x_\delta} \right) \Delta x_\delta = 0$. Thus, because $\Delta x_\delta = \Delta a_\delta$ is constant in V_{II} and C, the released energy G^* becomes

$$G^* = J_\delta \Delta x_\delta \qquad (17)$$

where

$$J_\delta = \int_C \left(W\delta_{\delta\beta} - \sigma_{\alpha\beta} \frac{\partial u_\alpha}{\partial x_\delta} \right) \tilde{n}_\beta d\tilde{S}$$

$$+ \int_{V_{II}} \left(\sigma_{\alpha\beta} \frac{\partial \hat{\theta}_{\alpha\beta}}{\partial x_\delta} - f_\alpha \frac{\partial u_\alpha}{\partial x_\delta} \right) dV \quad . \qquad (18)$$

In the absence of body forces, the J_1 component of Eq. (18) was derived previously by Ainsworth, et al (8). The surface integral term of Eq. (18) was derived for 2-D formulations by Eshelby (12) and Rice (1), and for 3-D formulations by Knowles and Sternberg (13).

The formulations of energy release rate (12), and modified J-integral (18) are strictly valid for hyperelastic materials, with the stress state given by Eq. (7). In applications of these techniques, elastic-plastic material behavior can be modeled by deformation plasticity theory when unloading and severe departure from proportional loading are restricted to a small region of the structure. If thermal as well as mechanical loads are present, a greater potential exists for violating these restrictions on the loading path. Thus, care must be exercised in applying the theory to combined loading situations.

In applications described below, the energy release rate G_T and the modified J-integral are evaluated numerically using results obtained from conventional finite element analyses. For three-dimensional calculations of G_T, the area increment ΔA covered by the virtual crack extension is computed from conventional finite element isoparametric interpolating functions (14).

NONLINEAR ANALYSIS OF PRESSURE VESSEL

The virtual-crack-extension technique was applied to semi-elliptical surface cracks in an experimental test vessel (identified in (15) as intermediate test vessel ITV V-8A) under elastic-plastic conditions. The vessel will be used in laboratory tests to validate analytical and computational techniques for ductile fracture analysis of part-through cracks in pressure vessels (15). The cracked region of the test vessel is designed to have low upper shelf fracture toughness in order to investigate the effects of this phenomenon on some older reactor pressure vessels subjected to radiation in service. Three-dimensional finite element analyses were performed for a range of crack depths and internal pressures using a deformation plasticity material model. Energy release rates computed from these analyses were compared with available tearing resistance data to estimate the onset of stable tearing as well as unstable tearing of the crack.

Figures 4 and 5 show the dimensions of a quarter section of the test vessel as modeled and a portion of the finite element discretization used in the plane of the crack. Analyses were performed for five crack configurations possessing the same ratio of depth to half-length, a/b = 2/3, with the depth varying from a = 90 mm to a = 100 mm (see Table 1). These finite element models, as well as those described in the next section, were produced by the ORMGEN mesh generating program (16). Each of the five models consists of 1678 nodes and 303 isoparametric brick elements, with six element divisions around the crack front. The detail of the crack tip (Fig. 5(b)) illustrates the collapsed prism elements with midside nodes that allow for a 1/r singularity at the crack front (17). In the collapsed elements, the nodes that initially share the same locations at the tip will separate with increasing load to allow for blunting of the crack.

The material response was modeled using deformation plasticity theory (18) and a multi-linear

Table 1. Dimensions of Semi-Elliptical Surface Cracks

Model	a(mm)	b(mm)
1	90.0	135.0
2	92.5	138.75
3	95	142.5
4	97.5	146.25
5	100.0	150.0

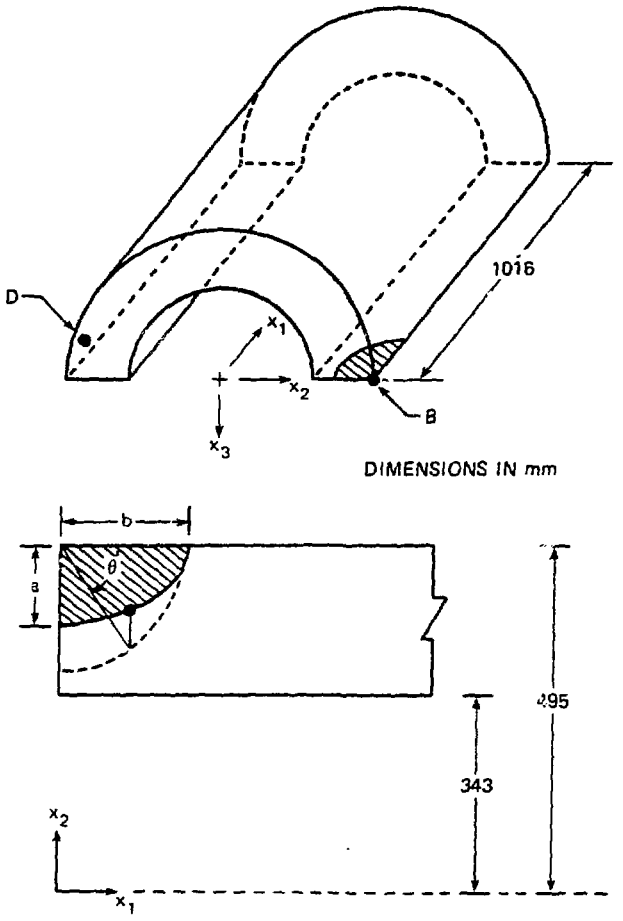

Fig.4 Description of ITV V-8A cylinder analyzed showing crack and quarter cylinder as modeled.

approximation to the experimental uniaxial stress-strain curve depicted in Figure 6. This material model was implemented in the Oak Ridge version of the finite element structures program ADINA (19), which was the application program for the analyses described below. For the five models that were analyzed, material properties were taken to be Young's modulus E = .2096 x 10^5 MPa, Poisson's ratio ν = 0.3 and initial yield stress σ_y = 427.5 MPa.

In the analysis of each model, the pressure load p was applied in six steps, from p = 105 MPa to p = 163 MPa (see Table 2). Figure 7 depicts the variation of crack mouth opening displacement (CMOD) with pressure in the axial symmetry plane at the outer surface (location B in Figure 4). The variation of hoop strain ε_h with pressure near the outer surface at a point removed from the crack (location D in Figure 4) is shown in Figure 8. The variations of hoop strain among the five models are not discernible on the scale of these plots. Measured data for CMOD and hoop strain will be recorded near locations B and D, respectively, for the laboratory test of the vessel.

For the five models, results from the ADINA analyses were post-processed to evaluate numerically the variations of the energy release rate G_T, Eq. (12), along the crack front. For Model 1 (a = 90 mm), Figure 9 depicts the variation of G_T with elliptic angle θ (measured from the surface) with pressure p taken as

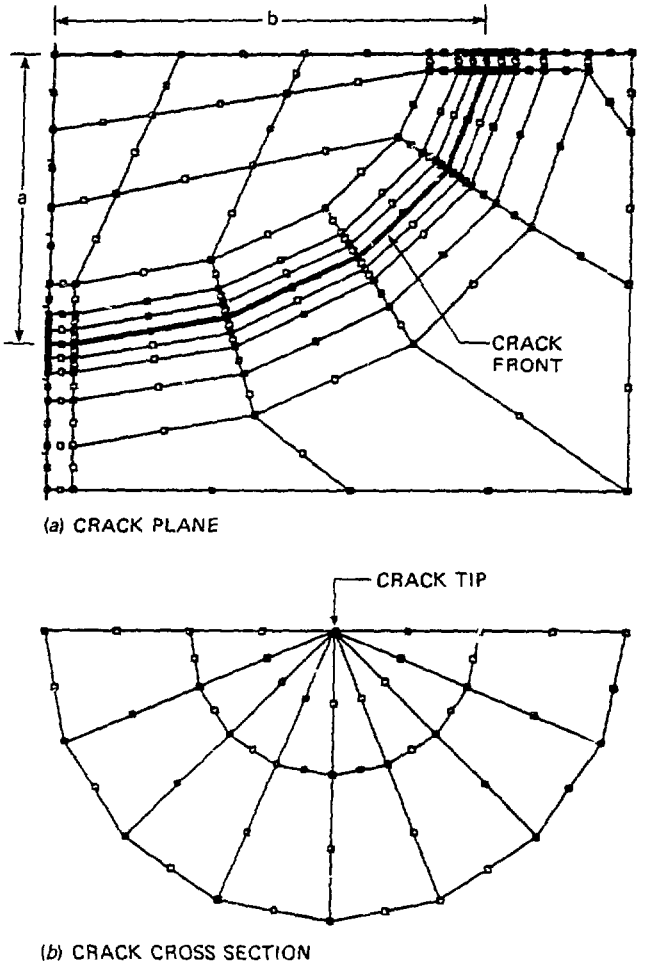

Fig.5 Detail of finite element model of intermediate test vessel

(a) Crack plane
(b) Crack cross section

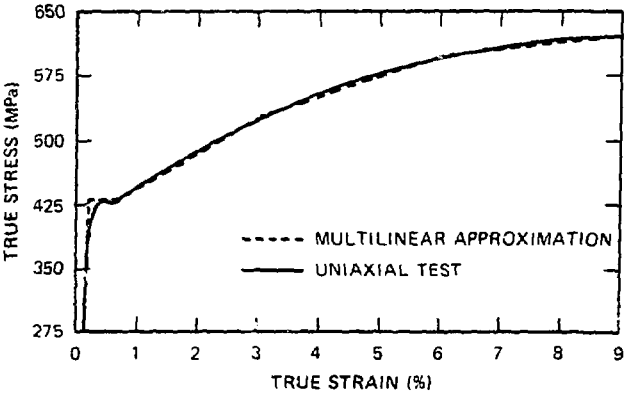

Fig.6 Uniaxial stress-strain curve for intermediate test vessel V-8A material

Table 2. Pressure Loads for Analyses of Semi-Elliptical Surface Cracks

Load Step	Pressure (MPa)
1	105
2	120
3	140
4	155
5	160
6	163

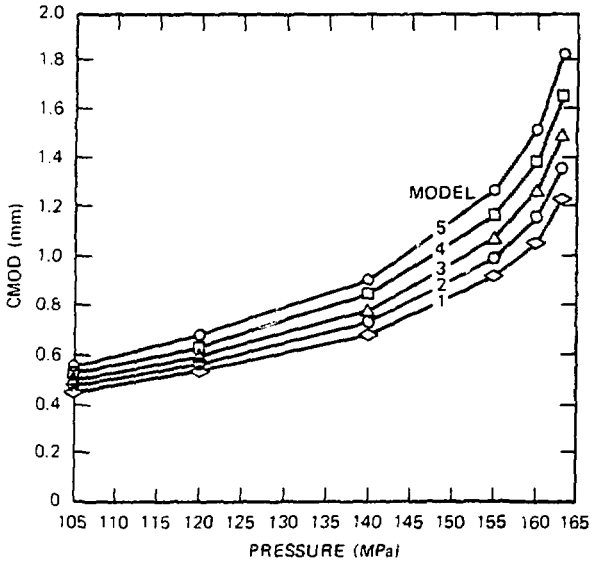

Fig.7 Variation of crack mouth opening displacement, CMOD, with pressure at point B (see Fig. 4)

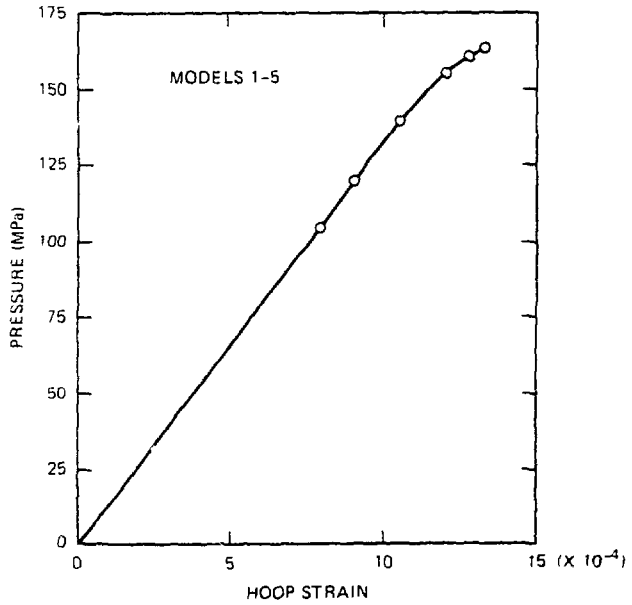

Fig.8 Variation of hoop strain, ε_h, with pressure at point D (see Fig. 4)

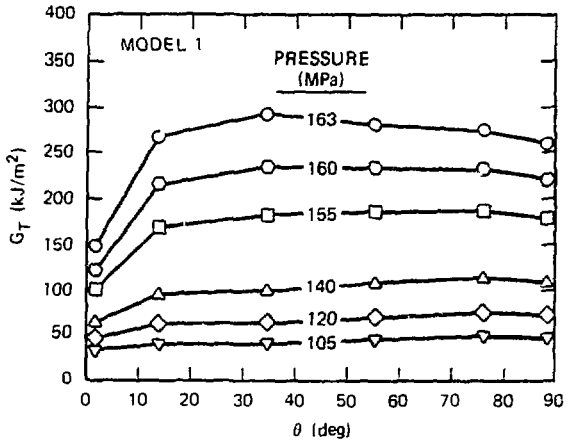

Fig.9 Variation of energy release rate, G_T, along crack front for model 1

a parameter. The curves showing G_T versus pressure p are plotted in Figure 10 for the same model, with the angle θ taken as the parameter. Analogous results for Model 5 (a = 100 mm) are given in Figures 11 and 12; results (not shown here) for the remaining three models fall in the range defined by those for models 1 and 5.

The energy release rate values computed for the five cracks were used to generate conventional J_A versus Δa crack growth curves for a set of pressure loads, illustrated in Figure 13. For a given pressure load, the curve was constructed by recording the maximum G_T value along the crack front for each of the five crack depths (from a = 90 mm to a = 100 mm) and setting $J_A = G_T$ at a. The behavior of a crack is assumed to be determined by the magnitudes and slopes of the J_A curves relative to the magnitudes and slopes of a tearing resistance (J_R) curve. The tearing resistance J_R is an intrinsic property of the material determined by tests of fracture mechanics specimens.

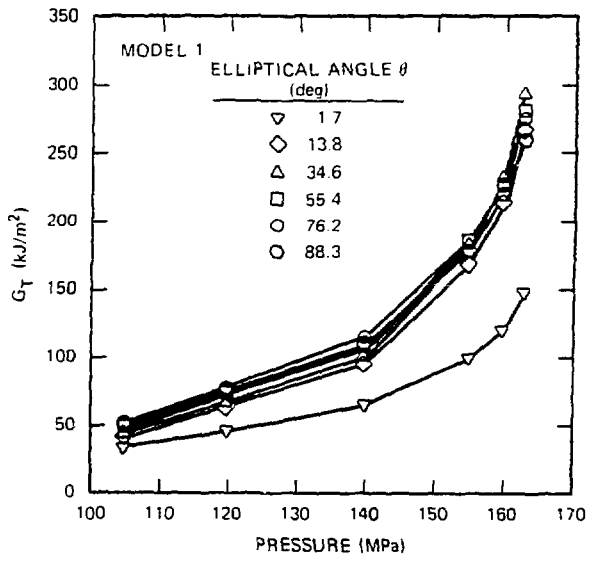

Fig.10 Variation of energy release rate, G_T, with pressure for model 1

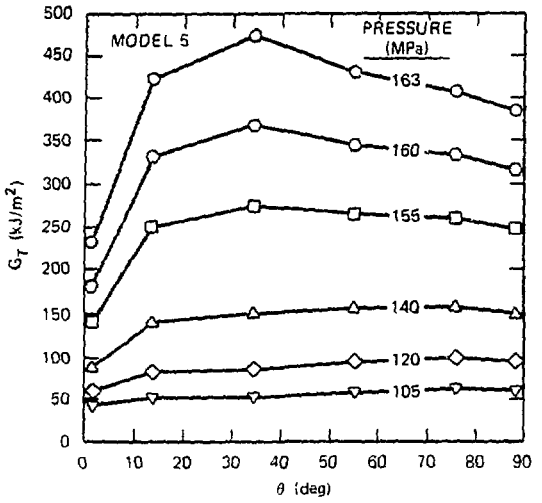

Fig.11 Variation of energy release rate, G_T, along crack front for model 5

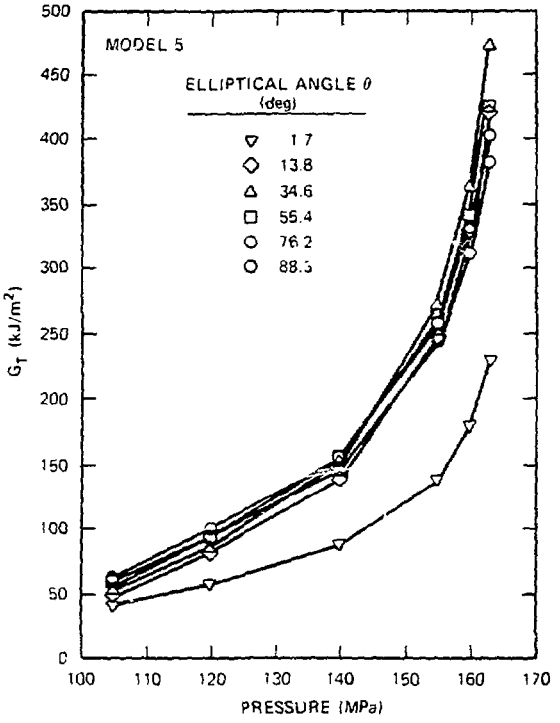

Fig.12 Variation of energy release rate, G_T, with pressure for model 5

Indicated in Figure 13 are tearing resistance curves represented by a power law, $J_R = 157.0\ (\Delta a)^{0.28}$, where $\Delta a = a - a_o$, for two initial crack depths, a_o = 90 mm and a_o = 92.5 mm. The parameters in this relation were obtained from fracture test data (20) compiled for the material in the cracked region of the vessel. A value of tearing initiation toughness, J_{Ic} = 115 kJ/m^2, was also measured.

A crack of given initial depth, e.g., a_o = 90 mm, will be subcritical until the pressure is increased to the point that $J_A = J_{Ic}$, a critical value observed in J_R tests. For J_A less than J_{Ic}, the crack tip is blunting, which results in a slight forward displacement of the crack tip with no tearing. Physical tearing ensues when pressure p is increased to the point that $J_A(p,a) = J_{Ic}$, where Δa satisfies the relation $J_R(\Delta a) = J_{Ic}$ (point L in Figure 13). Thereafter, stable tearing will progress with increasing load, as determined by $J_A = J_R$, until a load is reached for which a further infinitesimal extension of the crack would result in $J_A > J_R$ (point M). At this unstable tearing load, the J_R curve is tangent to a J_A curve. In Figure 13, the tearing initiation and instability points for a crack having an initial depth a_o = 92.5 mm are identified as points N and O, respectively.

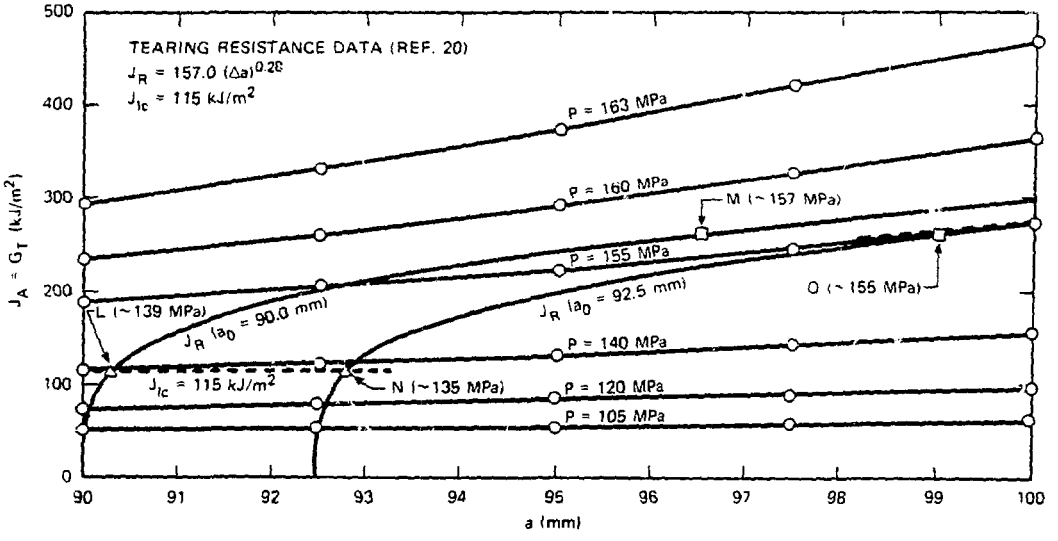

Fig.13 J_A and J_R curves for nonlinear analysis of intermediate test vessel V-8A using resistance curve data from Ref. 20

PRESSURIZED-THERMAL-SHOCK ANALYSIS

The second application is a thick-walled cylindrical test vessel (ITV) subjected to combined pressure and thermal-shock loading. The vessel will be used in pressurized-thermal-shock (PTS) studies (7) designed to validate analytical and computational fracture techniques applicable to pressurized water reactor (PWR) vessels under combined thermo-mechanical loading. For these tests, material properties and pressure-temperature transients will be selected to produce fracture toughness and stress gradients in the crack region that are representative of a PWR vessel under accident conditions.

In preparation for the PTS analysis of the test vessel, the energy release function G*, modified for thermal strains according to Eq. (11), and the J-integral, similarly modified according to Eq. (18), were applied to a thermally loaded center-cracked plate with a known solution. The plate was subjected to a parabolic temperature distribution $T = \Delta T\,(x_1/w)^2$ and analyzed under 2-D thermo-elastic plane stress conditions; here x_1 is measured from the crack center in the plane of the crack and w is the half-width of the plate. If b denotes the half-length of the crack, the known solution (8) for the stress intensity factor is given by $K_I = 0.5547E\alpha\Delta T(b)^{1/2}$ where α is the thermal expansion coefficient, and E the elastic modulus. A 2-D energy release rate calculation using Eq. (12) yielded $K_I = \sqrt{G_I E} = 0.5568E\alpha\Delta T(b)^{1/2}$, for a 0.4% difference from the known solution. The same result (to four significant digits) was obtained from application of the modified J-integral, Eq. (18), and $K_I = \sqrt{J_1 E}$, where J_1 was averaged from twelve contours around the crack tip.

These techniques were then applied to the test vessel under combined pressure and thermal- shock loading, as shown in Figure 14. The cylinder and liquid inside and outside are initially at uniform temperature $T_o = 100^oC$. In this condition and with zero pressure, the cylinder is free of stress. At time t = 0, the temperature of the outside liquid undergoes a step change $\Delta T_o = -290^oC$ and an internal pressure p = 68.9 MPa is applied. As Figure 14(b) illustrates, two different crack configurations were considered: the end-to-end crack of uniform depth and the long but finite (i.e. less than end-to-end) crack. Temperature solutions (assuming an uncracked body) and linear thermo-elastic solutions for several time steps in the thermal transient were calculated from 2-D plane strain and from fully 3-D analyses. The solutions presented here are for time t = 4 min into the transient, when maximum K_I values were obtained.

The 2-D plane strain analyses were performed on an outside surface crack assumed to be of depth a = 64 mm. For comparison, an axially constrained 3-D model containing an end-to-end crack of the same uniform depth was also analyzed. From these solutions, K_I values were determined from Eqs. (12) and (18) with $K_I = \sqrt{G_I E'} = \sqrt{J_1 E'}$, $E' = E/(1-\nu^2)$. In Table 3, the computed K_I values at time t = 4 min are given for both the 2-D and 3-D solutions, and agree to within 2%. A slightly greater mesh refinement was used in the 2-D finite element model, permitting a more accurate resolution of the radial thermal gradient and, consequently, the thermal stresses.

Additional 3-D models of the test cylinder were analyzed to evaluate the applicability of the 2-D results to finite length cylinders with closed ends and with finite length cracks. To examine the effects of finite crack length, the 3-D model shown in Figure 14 was analyzed for a long but finite crack, with dimensions a = 64 mm and b = 450 mm. A second analysis

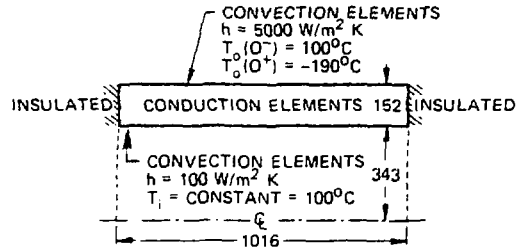

(a) BOUNDARY CONDITIONS FOR THERMAL ANALYSIS

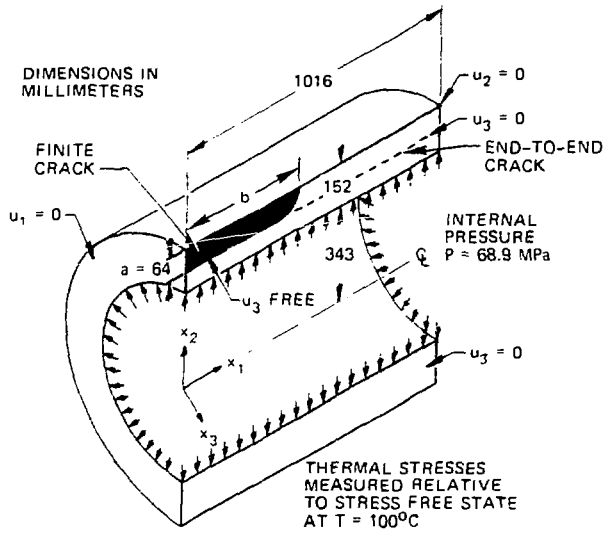

(b) BOUNDARY CONDITIONS FOR FRACTURE MECHANICS ANALYSIS

Fig.14 Problem definition and dimensions for pressurized thermal shock analysis of an intermediate test vessel

Table 3. Computed K_I (MPa $\sqrt{m}$) values for pressurized-thermal-shock of an ITV with an end-to-end crack (a/w = 0.42) on the outside surface (time = 4 min)

2-D modified J-integral:[1]	
Pressure only	109.3
Thermal only	190.3
Combined	299.6
2-D energy release rate G_I:[1]	
Pressure only	109.4
Thermal only	190.4
Combined	299.8
3-D energy release rate G_I:[2]	
Pressure only	107.8
Thermal only	186.9
Combined	294.7

[1] Two-Dimensional analyses assuming plane strain.

[2] Fully three-dimensional analyses, axially constrained.

was performed on an axially constrained 3-D model with an end-to-end crack of uniform depth a = 64 mm. The mesh refinement of the latter end-to-end crack model was comparable to that of the finite crack model in the direction of the thermal gradient (but coarser than the 3-D model of the same crack used for Table 3). Figure 15 shows the variation of K_I along the finite crack front (b = 450mm), computed from the energy release rate G_I of Eq. (12). The constant K_I value for the end-to-end crack is indicated in the same figure. For comparison, K_I values computed from application of an embedded-singularity hybrid-displacement technique (21) to the finite length crack model are also shown in Figure 15. For the finite crack, the variation of K_I from its maximum value is no more than 5% over a 200 mm segment of the crack. Furthermore, the maximum K_I value (located at the center $x = 0$) for the finite crack is about 3% less than the value calculated for the end-to-end crack. The maximum K_I values shown in Figure 15 are from 7% to 10% lower than the 2-D and 3-D values given in Table 3 for the same problem. This difference is due primarily to the substantially greater mesh refinement of the finite element models used in the computations of Table 3.

To estimate roughly the effect of finite cylinder length on the K_I distribution, three different boundary conditions were applied to the ends of the cylinder containing an end-to-end crack of uniform depth a = 64 mm. The case of fixed axial displacement, representing an end-to-end crack in a long cylinder, was referred to previously in the discussion of Figure 15. A radially constrained case was included to model approximately the effects of uncooled heads on the experimental vessel. The third case is that of free end conditions. Results from the virtual-crack-extension technique of the present study and from the hybrid-displacement procedure (21) are shown in Figure 16. The radially-fixed case, implying the presence of vessel heads, alters K_I near the ends but does not affect its value significantly at the center of the cylinder. In addition, the variation of K_I from its maximum value is less than 5% within 400 mm of the center.

The results depicted in Figures 15 and 16 and in Table 3 have implications for the applicability of 2-D analysis to PTS studies. The long but finite crack in the test vessel has a substantial segment over which the variation in K_I is no greater than the magnitude of uncertainty in fracture toughness. End conditions have little effect on K_I distribution near the center of the crack. Apparently, a long but finite crack can be represented adequately by the end-to-end crack for purposes of simplified parameter studies of PTS tests using less expensive 2-D analysis techniques. However, more costly 3-D analyses that incorporate elastic-plastic material response will eventually be required in the planning of some details of specific PTS experiments.

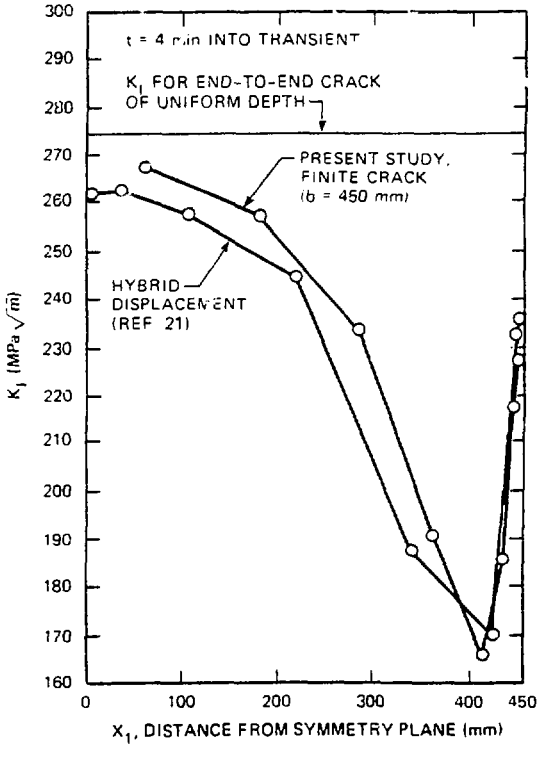

Fig.15 Linear elastic pressurized thermal shock analysis of an ITV with an outside finite length crack (b = 450 mm), t = 4 min into transient

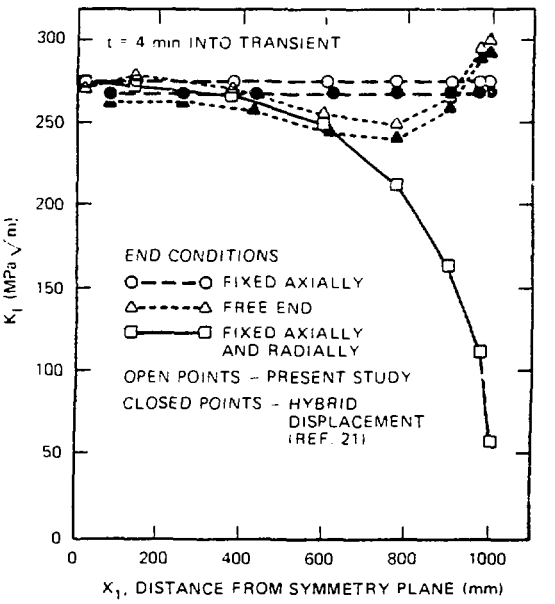

Fig.16 Linear elastic pressurized thermal shock analysis of an ITV with an outside end-to-end axial crack for three different end conditions

CONCLUSION

A modification to the energy release rate formulation of deLorenzi has been proposed to account for thermal strains in cracked bodies. The combined thermo-mechanical formulation is valid for thermo-elastic as well as deformation plasticity material models. The technique is better suited for calculating stress intensity parameters of 3-D crack configurations than the J-integral, which involves a difficult surface integral. Two applications of the technique were described in this study. In the first, the stability of semi-elliptical surface cracks in an experimental test vessel was analyzed with the finite element method and deformation plasticity theory. Energy release

rates computed from these analyses were compared with available tearing resistance data for two different initial crack depths. These comparisons were used to estimate pressure loads for the onset of stable tearing as well as unstable tearing of the cracks. The second application was a thick-walled test vessel subjected to combined pressure and thermal shock loading. Both 2-D and 3-D analyses were performed for surface cracks in the vessel to evaluate the applicability of 2-D techniques to finite length cylinders containing finite length cracks. Results indicate that 2-D analysis techniques are adequate for the preliminary design of pressurized-thermal-shock tests, but 3-D nonlinear analyses will be necessary for resolving specific details of the experiments.

ACKNOWLEDGMENT

This study was supported by the U. S. Nuclear Regulatory Commission through the Heavy Section Steel Technology program at the Oak Ridge National Laboratory, Oak Ridge, Tennessee. The Oak Ridge National Laboratory is operated by Union Carbide Corporation, Nuclear Division, for the U. S. Department of Energy under U. S. government contract W-7405 eng 26.

REFERENCES

1 Rice, J. R., "A Path Independent Integral and the Approximate Analysis of Strain Concentration by Notches and Cracks,"Journal of Applied Mechanics, Vol. 35, June 1968, pp. 379-386.

2 Hellen, T. K., "The Finite Element Calculations of Stress Intensity Factors Using Energy Techniques," 2nd International Conference on Structural Mechanics in Reactor Technology (SMiRT), Paper G5/3 Berlin, Germany, 1973.

3 Parks, D. M., "A Stiffness Derivative Finite Element Technique for Determination of Crack Tip Stress Intensity Factors," International Journal of Fracture, Vol. 10, No. 4, Dec. 1974, pp. 487-502.

4 DeLorenzi, H. G., "On the Energy Release Rate and the J-Integral for 3-D Crack Configurations," TIS Report 80CRD113, General Electric Company, Schenectady, N.Y., June 1980.

5 DeLorenzi, H. G., and Shih, C. F., "3-D Elastic-Plastic Investigation of Fracture Parameters in Side-Grooved Compact Specimens," TIS Report 80CRD211, General Electric Company, Schenectady, N.Y., Sept. 1980.

6 DeLorenzi, H. G., "3-D Elastic-Plastic Fracture Analysis with ADINA," Computers and Structures, Vol. 13, 1981, pp. 613-621.

7 Bryan, R. H., and Bryson, J. W., "Pressurized Thermal-Shock Stress and Fracture Analysis," Heavy Section Steel Technology Program Quarterly Progress Report for July-September 1981, NUREG/CR-2141/V3, (ORNL/TM-8145), Oak Ridge National Laboratory, Oak Ridge, TN, Feb. 1982, pp. 108-121.

8 Ainsworth, R. A., Neale, B. K. and Price, R. H., "Fracture Behaviour in the Presence of Thermal Strains," Report RD/B/N4152, Central Electricity Generating Board, Research Division, Berkeley Nuclear Laboratories, Nov. 1977.

9 Wilson, W. K., and Yu, I. W., "The Use of the J-Integral in Thermal Stress Crack Problems," International Journal of Fracture, Vol. 15, No. 4, Aug. 1979, pp. 377-387.

10 Griffith, A. A., "The Phenomena of Rupture and Flows in Solids," Philosophical Transactions of the Royal Society, Ser. A221, London, 1920, pp. 163-198.

11 Griffith, A. A., "Theory of Rupture," Proceedings of the First International Congress for Applied Mechanics, Delft, 1924, pp. 55-63.

12 Eshelby, J. D., "The Continuum Theory of Lattice Defects," Solid State Physics, Academic Press, New York, Vol. 3, 1956, pp. 79-144.

13 Knowles, J. K., and Sternberg, E., "On a Class of Conservation Laws in Linearized and Finite Elastostatics," Archive for Rational Mechanics and Analysis, Vol. 44, No. 3, 1972, pp. 187-211.

14 Zienkiewicz, O. C., The Finite Element Method, 3rd. ed., McGraw-Hill, London, 1977.

15 Holz, P. P., and Bryan, R. H., "Intermediate Test Vessel V-8A," Heavy Section Steel Technology Program Quarterly Progress Report for April-June 1981, NUREG/CR-2141/V2, (ORNL/TM-7955), Oak Ridge National Laboratory, Oak Ridge, TN, Oct. 1981, pp. 71-74.

16 Bass, B. R., and Bryson, J. W., "Computational Methods in Three-Dimensional Nonlinear Fracture Mechanics," Heavy Section Steel Technology Program Quarterly Progress Report for July-September 1981, NUREG/CR-2141/V3, (ORNL/TM-8145), Oak Ridge National Laboratory, Oak Ridge, TN, Feb. 1982, pp. 3-9.

17 Barsoum, R. S., "Triangular Quarter-Point Elements as Elastic and Perfectly-Plastic Crack Tip Elements," International Journal for Numerical Methods in Engineering, Vol. 11, 1977, pp. 85-98.

18 Mendelson, A., Plasticity: Theory and Application, MacMillan, New York, 1968.

19 Bathe, K. J., "ADINA - A Finite Element Program for Automatic Dynamic Incremental Nonlinear Analysis," Report 82448-1, Massachusetts Institute of Technology, Cambridge, Mass., Sept. 1975 (revised Dec. 1978).

20 Domain, H. A., "Vessel V-8 Repair and Preparation of Low Upper-Shelf Weldment," Final Report, Contracts CRD-1055, CRD-1078, Babcox and Wilcox Company, Alliance, Ohio, Jan. 1982.

21 Atluri, S. N., Bass, B. R., Bryson, J. W., and Kathiresan, K., "ORFLAW: A Finite Element Program for Direct Evaluation of K-Factors for User-Defined Flaws in Plates, Cylinders and Pressure-Vessel Nozzle Corners," NUREG/CR-2494, (ORNL/CSD/TM-165), Oak Ridge National Laboratory, Oak Ridge, TN, April 1982.